Higgs Boson Search Sensitivity in the $H \to WW$ Dilepton Decay Mode at $\sqrt{s} = 7$ and 10 TeV

Edmond L. Berger^{a,}* Qing-Hong Cao^{a,b,}†

C. B. Jackson^{a,}‡ Tao Liu^{b,}§ and Gabe Shaughnessy^{a,c}¶

^{a}*High Energy Physics Division, Argonne National Laboratory, Argonne, IL 60439*

^{b}*Enrico Fermi Institute, University of Chicago, Chicago, IL 60637*

^{c}*Department of Physics and Astronomy, Northwestern University, Evanston, IL 60208*

Abstract

Prospects for discovery of the standard model Higgs boson are examined at center of mass energies of 7 and 10 TeV at the CERN Large Hadron Collider. We perform a simulation of the signal and principal backgrounds for Higgs boson production and decay in the W^+W^- dilepton mode, finding good agreement with the ATLAS and CMS collaboration estimates of signal significance at 14 TeV for Higgs boson masses near $m_H = 160$ GeV. At the lower energy of 7 TeV, using the same analysis cuts as these collaborations, we compute expected signal sensitivities of about 2 standard deviations (σ's) at $m_H = 160$ GeV in the ATLAS case, and about 3.6 σ in the CMS case for 1 fb^{-1} of integrated luminosity. Integrated luminosities of 8 fb^{-1} and 3 fb^{-1} are needed in the ATLAS case at 7 and 10 TeV, respectively, for 5 σ level discovery. In the CMS case, the numbers are 2 fb^{-1} and 1 fb^{-1} at 7 and 10 TeV. Our different stated expectations for the two experiments arise from the more restrictive analysis cuts in the CMS case. Recast as exclusion limits, our results show that with 1 fb^{-1} of integrated luminosity at 7 TeV, the LHC may be able to exclude m_H values in the range 160 to 180 GeV provided no signal is seen.

---

*Electronic address: berger@anl.gov

†Electronic address: caoq@hep.anl.gov

‡Electronic address: jackson@hep.anl.gov

§Electronic address: taoliu@theory.uchicago.edu

¶Electronic address: g-shaughnessy@northwestern.edu

I. INTRODUCTION

Discovery of the Higgs boson of electroweak symmetry breaking is a prime goal of experimental investigations at the CERN Large Hadron Collider (LHC). Considerable efforts have been made by the ATLAS and CMS collaborations to simulate the production and decay of the standard model Higgs boson at the LHC's center-of-mass (cm) design energy of 14 TeV [1, 2], and estimates have been made of the integrated luminosity required to observe the Higgs boson and to measure its properties. The recent decision to begin operation of the LHC at the reduced cm energy of 7 TeV (and possibly 10 TeV) [3] motivates an examination of the discovery potential at these lower energies. In this paper we present our estimates of the potential for finding the Higgs boson through its W^+W^- decay mode at 7 TeV and 10 TeV.

At both the Fermilab Tevatron and the LHC the largest channel for production of the Higgs boson is gluon fusion, $gg \to HX$, with the ggH coupling arising via a top quark loop (cf. Refs. [4, 5]). The relative dominance of production and decay modes depends on the Higgs boson mass. A Higgs boson with mass $m_H \gtrsim 135$ GeV decays predominantly to W boson pairs with one of the W's potentially off mass-shell. In this mass range inclusive production through gluon fusion is dominant at the LHC, with the best sensitivity occurring around $m_H \approx 160 - 170$ GeV, where the WW decay mode is fully open.

In this paper we limit ourselves to the gluon fusion production process and to the WW decay mode, focusing on observation in the dilepton channel in which $H \to W^+W^- \to l^+l^-$ plus missing energy. We present a simulation of the signal and of the salient continuum W^+W^-, $t\bar{t}X$, and $W +$ jets backgrounds, applying the same analysis cuts used by the the ATLAS and CMS collaborations at 14 TeV [1, 2]. In the ATLAS case, we conclude that integrated luminosities of 8 fb^{-1} and 3 fb^{-1} are needed at 7 and 10 TeV, respectively, for 5σ level discovery of a standard model Higgs boson of mass $m_H = 160$ GeV in this production and decay mode. In the CMS case, the numbers are 2 fb^{-1} and 1 fb^{-1} at 7 and 10 TeV, respectively, for 5σ level discovery. Optimization of the analysis cuts for 7 and 10 TeV might reduce the required luminosities. The different analysis cuts explains the different required luminosities for the two experiments. Larger samples would be needed for masses as low as $m_H = 140$ GeV or above $m_H = 180$ GeV.

There are important production channels in addition to $gg \to H$. These include produc-

2

tion of the Higgs boson with an associated W boson, Z boson, or top quark pair, as well as production of the Higgs boson through vector-boson or bottom-quark fusion. A light Higgs boson ($m_H \lesssim 135$ GeV) decays predominantly to bottom quark pairs. In this case the inclusive Higgs boson signal is difficult to pick out from the large QCD $b\bar{b}$ background. Other important Higgs boson decay modes, both at the Tevatron and the LHC, are ZZ for high mass Higgs bosons, and tau meson pairs and photon pairs for low mass Higgs bosons. These and other modes were used in the recent combined fit of Tevatron data to exclude the mass range of $163\,\text{GeV} < m_H < 166\,\text{GeV}$ at 95% C. L. [6].

According to current expectations, the LHC will operate at 7 TeV for a couple of years or until it accumulates an integrated luminosity of $1\,\text{fb}^{-1}$ [3]. With low luminosity it might be difficult to observe a light Higgs boson owing to the small branching fraction to $\gamma\gamma$, or a heavy Higgs boson in the ZZ channel because this decay mode suffers from the small decay branching ratio of $Z \to \ell^+\ell^-$ ($\ell^\pm$ denotes charged leptons). Based on such considerations, we focus first on the leading decay channel $H \to WW$ throughout this work. We intend to address the ZZ case and other production and decay modes at a later date.

The remainder of the paper is organized as follows. In Section II we present next-to-leading order (NLO) calculations of the production cross section of the Higgs boson and the principal backgrounds at the LHC for 7, 10, and 14 TeV. We then describe our method for simulating the signal and the background processes, taking into account the different lepton momentum requirements and kinematic cuts used by the ATLAS and CMS collaborations. As shown in Section III, our determinations of signal and background acceptances at 14 TeV are in good agreement with those reported in the 2008 ATLAS Physics Performance Report (PPR) [1] and, except in the $t\bar{t}X$ case, also with the 2007 CMS PPR [2]. We examine possible interpretations of this one disagreement. In Section IV we use our acceptances and the NLO cross sections at lower LHC energies to determine the discovery potential at 7 and 14 TeV. A brief Section V addresses Higgs boson exclusion limits. We state our conclusions in Section VI.

II.   CROSS SECTIONS AND DETECTION EFFICIENCIES

For the $H \to WW$ channel, ATLAS [1] and CMS [2] present detailed studies of the signal and backgrounds at a cm energy of 14 TeV. The collider signature of the signal events is

characterized by two oppositely-charged leptons plus large missing energy originating from two invisible neutrinos. The background processes include $t\bar{t}X$, WW, WZ, ZZ, Z+jets, and W+jets. Isolated leptons from heavy-flavor pair production and semi-leptonic decay are also generally important [7, 8]. After suitable cuts [7, 8], however, the background for $m_H > 140$ GeV is dominated by $t\bar{t}$ production and continuum W^+W^- pair production. In the following, we focus on these two backgrounds, but we also examine the potential role of W+jets which the ATLAS simulations suggest could be large, albeit with large uncertainties [1]. In this work, we represent the W+jets contribution by $W + c$ production, with $c \to lX$.

The ATLAS and CMS studies include sophisticated simulations of both signal and background event rates and also simulations of the detector response (e.g., lepton triggers and jet vetoes along with their associated efficiencies). In this paper, we follow a more simplified approach. An important check of our method is a comparison of our results for calculated acceptances and signal significance at 14 TeV with those of ATLAS and CMS. In this section, we first present our NLO calculations of the inclusive cross sections for the signal and principal backgrounds, and then we outline the algorithm used to generate both signal and background events for the comparison at 14 TeV and for our predictions at 7 and 10 TeV.

A.   Next-to-leading Order Cross Sections

The Higgs boson production cross section in gluon-gluon scattering has been calculated at leading order, next-to-leading order (NLO) [9] and next-to-next-to-leading order (NNLO) [10–12] in the infinite-top-quark-mass limit, and at LO and NLO [13, 14] with full top quark mass dependence. In addition to the QCD corrections, the NLO electroweak (EW) corrections have also been considered in the infinite-top-quark-mass limit [15], and more complete calculations have been performed by including light quark and top quark effects [16, 17]. Recently, the effects of the combined QCD and EW corrections were analyzed [18, 19].

We use the MCFM [20] code to compute the NLO inclusive cross sections for the signal and for background processes. The renormalization and factorization scales are set to m_H for the $gg \to H$ signal, to m_t for $t\bar{t}X$, to $2m_W$ for the WW continuum and to m_W for the WcX backgrounds. All cross sections are computed with the CTEQ6.6M parton distribution function (PDF) package [21]. In Table I, we present the NLO signal cross sections for

TABLE I: Inclusive NLO cross sections (pb) for Higgs boson production and the $t\bar{t}$, WW and Wc (both W^+c and W^-c) backgrounds.

process		14 TeV		10 TeV		7 TeV	
		LO	NLO	LO	NLO	LO	NLO
	$m_H = 140\,\mathrm{GeV}$	11.3	25.7	6.33	14.3	3.25	7.36
$gg \to H$	$m_H = 160\,\mathrm{GeV}$	9.16	20.6	5.01	11.2	2.51	5.62
	$m_H = 180\,\mathrm{GeV}$	7.59	16.9	4.07	9.04	1.99	4.42
	$m_H = 200\,\mathrm{GeV}$	6.44	14.2	3.39	7.47	1.62	3.57
$t\bar{t}$	$m_t = 175\,\mathrm{GeV}$	544	807	257	374	112	158
WW	$m_W = 80.3\,\mathrm{GeV}$	83.1	115	52.8	71.9	31.5	42.5
Wc	$m_W = 80.3\,\mathrm{GeV}$	6350	8450	3710	5000	2030	2720

several values of the Higgs boson mass ($m_H = 140, 160, 180$ and 200 GeV) and for the major backgrounds.

In Fig. 1(a), we show the total cross section for the signal as a function of the Higgs boson mass for several cm energies. Involving two gluons in the initial state, the signal cross section drops rapidly with decreasing cm energy as can be easily understood from a consideration of the behavior of the gluon PDF. The Higgs boson mass provides a natural choice of the physics scale resulting in an effective parton Bjorken-x, $\langle x \rangle \simeq m_H/\sqrt{s}$. For a given Higgs boson mass, lowering the cm energy increases the effective x. Numerically, $\langle x \rangle \simeq m_H/\sqrt{s} \sim 0.01$ for a 140 GeV Higgs boson at 14 TeV and $\langle x \rangle \simeq m_H/\sqrt{s} \sim 0.02$ at 7 TeV. Since the gluon PDF drops rapidly with x, the signal cross section also decreases rapidly as $\sqrt{s}$ is decreased, as shown in Fig. 1(a). Correspondingly, increasing the Higgs boson mass at fixed $\sqrt{s}$ will force the effective x to be larger, suppressing the cross section; see the broad band in the range 400 GeV $< m_H <$ 1000 GeV. To make the point clear we plot in Fig. 1(b) the ratio $R(= \sigma_i/\sigma_{14})$, defined as the ratio of the Higgs boson production cross section at a particular cm energy to the cross section at 14 TeV. We observe that the cross section is reduced by a factor of 2 to 2.5 at 10 TeV and by a factor of 3 to 8 at 7 TeV for a Higgs boson in the mass range of 100 GeV to 600 GeV.

The cross sections and the ratio R for the backgrounds are shown as a function of cm energy in Fig. 1(c) and (d). The $t\bar{t}$ background is produced mainly from the gluon-gluon
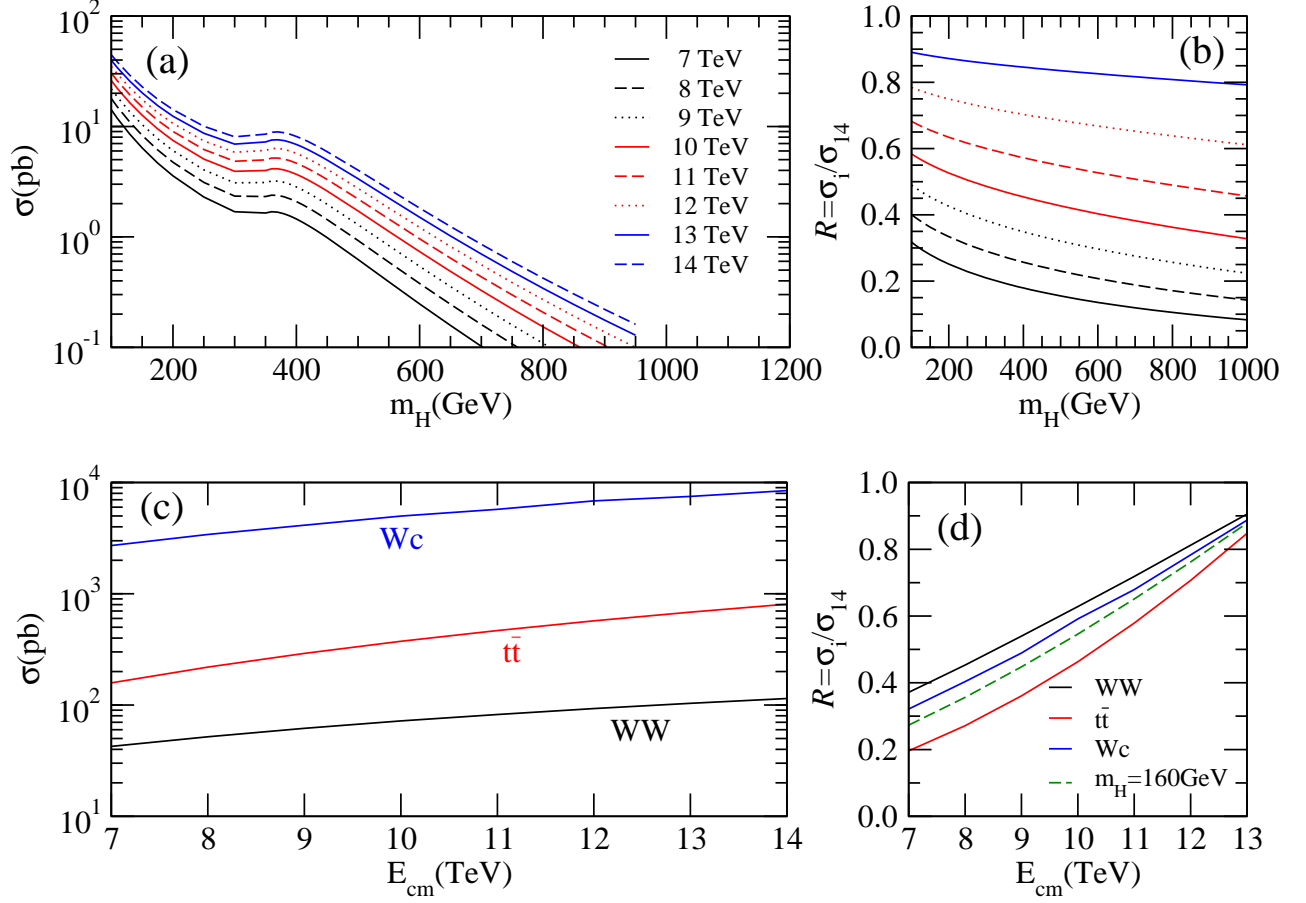
FIG. 1: (a) Total cross section for $gg \rightarrow H$ as a function of the Higgs boson mass for several different cm energies. (b) Ratio of the cross sections for $gg \rightarrow H$ at different cm energies to the cross section at 14 TeV. (c) Total cross sections for the backgrounds (W^+W^-, $t\bar{t}$ and Wc) as a function of the cm energy. (d) Ratio of the background cross sections at different cm energies to the cross sections at 14 TeV. For comparison we also plot the signal ratio curve for $m_H = 160$ GeV.

initial state at 14 TeV (90% from the gluon-gluon initial state and 10% from the quark-antiquark initial state). The gg initial state remains the leading contributor at 7 TeV (about 80%); see Fig. (3) in Ref. [22]. Therefore, lowering the cm energy decreases the $t\bar{t}$ background about as much as the Higgs signal; for example, $R(H) \approx R(t\bar{t}) \simeq 0.45$ and 0.20 at 10 TeV and 7 TeV for $m_H = 2m_t = 350$ GeV. On the other hand, the WW continuum background originates from the valence-quark and sea-quark initial state, and it decreases less than the signal and the $t\bar{t}$ background; see Fig. 1(c) and (d). This difference is crucial for the Higgs boson search. Since the WW continuum is the major background, the fact

that the signal is suppressed more than the background at lower cm energy means that more integrated luminosity is needed to restore the same significance for Higgs boson discovery as at 14 TeV. The Wc contribution is produced dominantly by $gs \to Wc$ with a hard scale of roughly m_W which leads to a typical parton-x where PDF suppression is not strong.

B. Generation of Event Samples

The Higgs boson signal at the LHC consists of the leading-order (LO) process $pp \to H \to WW$ along with higher-order corrections from initial-state radiation which can produce multiple jets. In order to simulate these effects, one may use event generators which include parton showering (such as PYTHIA [23] or HERWIG [24]) to generate event samples for both signal and backgrounds. In some cases, next-to-leading order (NLO) event generators which correctly account for NLO QCD effects and initial-state radiation are available (e.g., MC@NLO [25, 26] and POWHEG [27]). In most cases a p_T-dependent K factor obtained from a code such as MCFM is applied to the PYTHIA events in order to reweight the sample [1, 2].

In this work, we adopt a slightly simplified approach to model total event rates and parton showering effects. We generate the signal events with MadGraph/MadEvent [28], while we use ALPGEN [29] to generate the background events. This is done in an attempt to streamline the analysis since the matrix-elements-squared for the background processes are hard-coded in ALPGEN and, thus, are much more compact than those produced with MadGraph. However, for the signal processes, ALPGEN does not currently include spin-correlation effects among the leptons from $H \to W^+W^- \to \ell^+\nu\ell^-\bar{\nu}$. We choose to use MadGraph/MadEvent to produce events for the signal since spin-correlation effects are crucial for light Higgs boson searches [30, 31]. At leading order, the signal process is:

$$pp \to H \to W^+W^- \to \ell^+\nu\ell^-\bar{\nu} \,, \tag{1}$$

while the irreducible background process is:

$$pp \to W^+W^- \to \ell^+\nu\ell^-\bar{\nu} \,, \tag{2}$$

and the two reducible background processes are:

$$pp \to t\bar{t} \to W^+W^-b\bar{b} \to \ell^+\nu\ell^-\bar{\nu}b\bar{b} \,, \tag{3}$$

$$pp \to Wc \to \ell\nu c \,, \tag{4}$$

where the renormalization and factorization scales in all processes are chosen in accordance with the values mentioned in the previous section.

The reducible background from $t\bar{t}$ occurs when both b-quarks are not tagged as jets. The background of Wc masks the signal topology when the c-jet decays semi-leptonically to a tagged lepton. We assume an isolated lepton probability of $\epsilon_{c\to\ell} = 0.5\%$ when the c-quark is in the region $p_T > 20$ GeV and $|\eta| < 1$ [7, 8]. The momentum imparted to the isolated lepton is roughly 90-95% of the parent heavy flavor quark [7, 8]. The ATLAS collaboration includes the possibility of light jets faking isolated leptons near the level of few$\times 10^{-5}$. However, owing to the gluon PDF, the $gs \to Wc$ subprocess is enhanced, and the subsequent dilepton rate dominates the total $W^{\pm}$+jets rate. Therefore, we only consider $W^{\pm}c$ events and do not include light jet fakes.

To mimic the effects of initial state radiation and parton showering, we include the possibility of additional jets in the final state. For example, in addition to the LO signal process of Eq. (1), we also generate events for:

$$pp \to H + nj \to W^+W^- + nj \to \ell^+\nu\ell^-\bar{\nu} + nj \,, \tag{5}$$

where $n = 1$ or 2 and j denotes a light jet. The events from these processes are then combined with those of the LO process, and the sum is normalized to the total NLO event rate (we use inclusive K factors derived from the cross sections shown in Table I) to produce an effectively "showered" final state. Similarly, for the backgrounds, we add to the processes of Eqs. (2-4) events from:

$$pp \to W^+W^- + nj \to \ell^+\nu\ell^-\bar{\nu} + nj \,, \tag{6}$$

$$pp \to Wc + nj \to \ell\nu c + nj \,, \tag{7}$$

and:

$$pp \to t\bar{t} + nj \to W^+W^-b\bar{b} + nj \to \ell^+\nu\ell^-\bar{\nu}b\bar{b} + nj \,. \tag{8}$$

respectively, where $n = 1$ or 2 for $t\bar{t}$ and W^+W^- while $n = 1, 2, 3$ or 4 for $W^{\pm}c$. We reweight the total event rate in each case to the NLO value. At the level of event generation, we apply minimal threshold cuts. In the CMS case, we reject events with jets that fall in the range $p_T^j < 10$ GeV and $|\eta^j| < 2.5$, and in the ATLAS case, we reject events with jets that have $p_T^j < 15$ GeV and $|\eta^j| < 4.8$. The cut on p_T^j serves to eliminate collinear divergences.

TABLE II: Kinematic and physics cuts utilized by the ATLAS [1] and CMS [2] collaborations for the Higgs boson search in the process $gg \to H \to W(\to \ell\nu)W(\to \ell\nu)$. The SM backgrounds (BKGDs) considered are shown in the second row. Preselection cuts on the two charged leptons and further physics cuts are presented in the third and fourth rows, respectively. Here, $m_{\ell\ell}$ denotes the invariant mass of the two charged leptons, $\phi_{\ell\ell}$ is the angle in the transverse plane between the two charged leptons, $\not{E}_T$ is the missing transverse momentum, p_T is the transverse momentum, and η is the rapidity. The cluster transverse mass of the $(\ell\ell, \not{E}_T)$ system is defined as $M_T^C \equiv \sqrt{p_T^2(\ell\ell) + m^2(\ell\ell)} + \not{E}_T$.

	ATLAS [1]	CMS [2]
BKGDs	$t\bar{t}$ WW W+jets Single t $Z \to ll$	$qq/gg \to WW \to ll$ $t\bar{t} \to WWbb \to ll$ $tWb \to WWb(b) \to ll$ $ZW \to lll$ $ZZ \to ll$
Preselection	Two leptons with opposite charge with $p_T > 15$ GeV and $|\eta| < 2.5$ (crack region $1.37 < |\eta| < 1.52$)	Two tagged leptons with opposite charge with $p_T > 20$ GeV and $|\eta| < 2$
Physics Cuts	$12\,\text{GeV} < m_{ll} < 300\,\text{GeV}$ $\not{E}_T > 30$ GeV $Z \to \tau\tau$ veto with $|m_{\tau\tau} - m_Z| < 25\,\text{GeV}$ No jets with $p_T > 20\,\text{GeV}$ and $|\eta| < 4.8$, No b-jets with $p_T > 15\,\text{GeV}$ $\Delta\phi_{ll} < \pi/2$ and $M_T^C < 600\,\text{GeV}$	$\not{E}_T > 50$ GeV $\Delta\phi_{ll} < \pi/4$ $12\,\text{GeV} < m_{ll} < 40\,\text{GeV}$ No jets with $p_T > 15\,\text{GeV}$ and $|\eta| < 2.5$ $30\,\text{GeV} < \max\{p_T^{l1}, p_T^{l2}\} < 55\,\text{GeV}$ $25\,\text{GeV} < \min\{p_T^{l1}, p_T^{l2}\}$

We model detector resolution effects by smearing the final state energies according to:

$$\frac{\delta E}{E} = \frac{a}{\sqrt{E/\text{GeV}}} \oplus b \tag{9}$$

where we take $a = 10\%$ (50%) and $b = 0.7\%$ (3%) for leptons (jets).

III.   COMPARISONS WITH ATLAS AND CMS PPR RESULTS AT $\sqrt{s} = 14$ TEV

In this section we compare our expectations with those presented by ATLAS and CMS at 14 TeV, focusing on the experimental cuts and their acceptances. All of the cross sections in this section include the decay branching fraction of the Higgs boson into a pair of W bosons and their subsequent leptonic decays. They are summed over two flavors of leptons (e and μ) from $W \rightarrow l\nu$, unless specified otherwise.

Somewhat different preselection and physics cuts are chosen by ATLAS [1] and CMS [2] in order to suppress the standard model (SM) backgrounds. These are summarized here in Table II. The cuts are motivated by the different kinematic distributions of the signal and the backgrounds. The cut on missing energy rejects backgrounds like Drell-Yan production of a Z boson with $Z \rightarrow \ell^+\ell^-$, which have little or no intrinsic $\not{E}_T$. Both the signal and the $t\bar{t}$ and WW backgrounds exhibit large missing transverse energy associated with the momentum carried off by neutrinos. We display our calculations of the signal and background distributions in Fig. 2(a). The lower cut on the invariant mass of two charged leptons removes background from charmed and bottomed mesons, like J/ψ and Υ. The azimuthal angle cut $\Delta\phi_{\ell\ell}$ is valuable for a relatively light Higgs boson where the spin correlation of the two W-bosons plays an important role [32], as shown in Fig. 2(b). The backgrounds favor a large $\Delta\phi_{\ell\ell}$ whereas the signal populates small $\Delta\phi_{\ell\ell}$. As the Higgs boson mass increases, the separation between signal and background in $\Delta\phi_{\ell\ell}$ is not as strong.

A.   ATLAS comparison

The ATLAS PPR presents the prospects for Higgs boson searches in the $gg \rightarrow HX$ channel with subsequent Higgs boson decay $H \rightarrow WW \rightarrow e\mu\nu\nu$. They include both $e^+\mu^-$ and $e^-\mu^+$ [1], but not the same flavor combinations, $\mu^+\mu^-$ and e^+e^-. In this subsection we compare our simulation to the results in the ATLAS report. As a prelude, we first attempt to understand all the factors that enter in the event rates quoted by ATLAS.

ATLAS states that the average efficiency to reconstruct an electron candidate in the $gg \rightarrow H \rightarrow WW$ signal events is about 60% (before the p_T, η and isolation cone size ΔR cuts). The average efficiency to reconstruct a muon candidate is about 94.4%. Then kinematic cuts for both electron and muon of $p_T > 15\,\mathrm{GeV}$ and $|\eta| < 2.5$, and the calorimeter
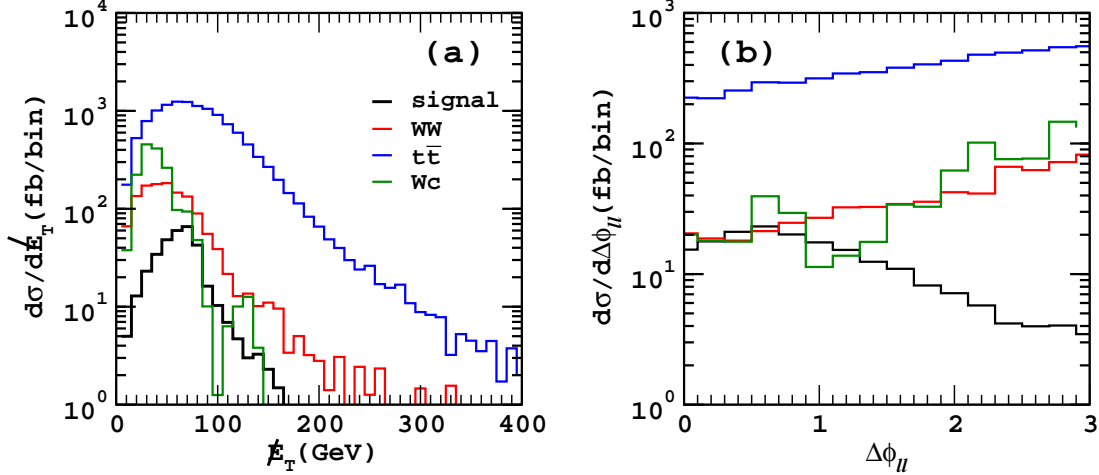
FIG. 2: Kinematic distributions of $\not{E}_T$ and $\Delta\phi_{\ell\ell}$ for a 160 GeV Higgs boson with $\sqrt{s} = 14$ TeV, where the black (red, blue,green) curves denote the signal (WW, $t\bar{t}$, Wc) contributions. Here, ATLAS-motivated lepton preselection cuts on p_T and η as well as the $m_{\ell\ell}$ cut are imposed.

ΔR isolation requirement, yield a further net suppression of 83.3% and 81.7% for electrons and muons, respectively. Starting from a NLO cross section for $pp \to H \to WW$ via gluon fusion for a Higgs boson mass $m_H = 170$ GeV of 19150 fb and using the efficiencies mentioned above, one can reproduce the entry of "lepton selection + $m_{\ell\ell}$" for $gg \to H$ in Table 3 of ATLAS report,

$$
\begin{aligned}
&\sigma(gg \to H \to WW \to e\mu) \\
&= 19150\,\text{fb} \times \frac{2}{81} \times (0.6 \times 0.944) \times (0.833 \times 0.817) \times 0.9 = 166.13 \text{ fb.} \quad (10)
\end{aligned}
$$

The factor 0.9 represents the effect of the cut on the dilepton invariant mass.

In obtaining our final numbers, we adopt the average efficiencies of 60% and 94.4% that ATLAS supplies for electron and muon reconstruction. We have no way to compute these. However, we calculate the effects of all other preselection and physics cuts. Table III displays the cut acceptances from our simulation along with the ATLAS results. We show results for the Higgs boson signal and the backgrounds. The cuts are defined in Table II. After all cuts, we obtain very good agreement with the ATLAS study for both signal and backgrounds at 14 TeV for $m_H = 170$ GeV.

Based on our calculations of the signal and background rates, and applying the ATLAS motivated cuts described above, we compute a signal significance $S/\sqrt{B} = 4.9$ for $m_H = 170$ GeV. This value is in good agreement with the number 4.5 quoted by ATLAS [1]. We

11

TABLE III: Cut acceptance for $m_H = 170\,\text{GeV}$ for Higgs boson production via gluon fusion, with $H \to WW \to e\nu\mu\nu$, at 14 TeV. The kinematic cuts listed in each row are applied sequentially.

	$H + (0,1,2)j$		$t\bar{t} + (0,1,2)j$		$WW + (0,1,2)j$		$Wc + (0-4)j$	
	Our	ATLAS	Our	ATLAS	Our	ATLAS	Our	ATLAS
i.d. $+ m_{\ell\ell}$	100%	100%	100%	100%	100%	100%	100%	100%
$\not{E}_T$	89%	89%	88%	86%	71%	70%	57%	87%
$Z \to \tau\tau$	89%	88%	88%	80%	71%	68%	57%	72%
Jet veto	37%	37%	0.31%	0.23%	31%	33%	28%	36%
b veto	37%	37%	0.31%	0.11%	31%	33%	28%	36%
$\Delta\phi_{\ell\ell}$ and M_T^C	30%	30%	0.07%	$(0.04 \pm 0.03)\%$	12%	$(12 \pm 0.4)\%$	8%	$(18 \pm 18)\%$

understand this difference in terms of our somewhat smaller $W+$ jet background estimate.

B. CMS comparison

The CMS PPR presents the prospects for Higgs boson searches in the gluon fusion channel with subsequent Higgs boson decay $H \to WW \to \ell\ell\nu\nu$ where $\ell = e, \mu$ [2]. The leptons, whether electrons or muons, are required to have $p_T > 20\,\text{GeV}$ and $|\eta| < 2$. The CMS PPR does not show cut acceptances for individual cuts, limiting our ability to make as detailed a comparison as we do for ATLAS. We find good agreement between our simulation and the CMS results after all cuts are imposed, except in the case of the $t\bar{t}$ background where our value is about a factor of 3.5 below that of CMS. This difference may arise from the lower jet transverse-momentum threshold taken by CMS. In the CMS case, we generate events with a cut at 10 GeV at the generator level, and then impose the 15 GeV cut at the event analysis level. These low values of the cuts may accentuate differences between our method and a full parton-showering. More is written on this discrepancy in the next subsection.

We do not include the loop-induced background $gg \to WW$ which was considered by CMS. At the level of σ_{total}, this channel makes a relatively small contribution to the continuum WW background (less than 5%). However, as shown in the CMS PPR, $gg \to WW$ contributes nearly 25% of the WW rate after all cuts are applied. The reason for the enhanced contribution after cuts is that the gg subprocess produces a different configuration

TABLE IV: Comparison to the CMS study for $m_H = 170\,\text{GeV}$ at 14 TeV.

	$H + (0,1,2)j$		$t\bar{t} + (0,1,2)j$		$WW + (0,1,2)j$	
	Our	CMS	Our	CMS	Our	CMS
lepton selection	100%	100%	100%	100%	100%	100%
All cuts	9.6%	8.8%	0.016%	0.062%	1.16%	1.07%

in phase space from the $q\bar{q}$ subprocess. For instance, in the valence-sea $q\bar{q}$ subprocess, the PDF dependence tends to boost the WW pair to slightly higher rapidity, in contrast with the gg initial state which tends to produce the WW (via the loop induced background or the Higgs boson decay) in the central rapidity region. Therefore, cuts that select on the signal events weaken the rejection of the $gg \to WW$ subprocess.

A study of possible $W+$ jets backgrounds is not included in the CMS study reported in their PPR. The CMS lepton threshold cut, $p_T^\ell > 20$ GeV, is harder than ATLAS and is more efficient at removing soft leptons from heavy flavor quark decays in the Higgs boson mass range of interest here [7, 8]. Nevertheless, we find that the $W + c$ channel can provide a background comparable to (or even larger) than $t\bar{t}$. Our estimate of its contribution is included in our predictions of the Higgs boson search sensitivity at 7 TeV and 10 TeV, reported in Section IV.

C. From CMS to ATLAS

The disagreement of our estimated efficiency for the $t\bar{t}$ background with the CMS value may be contrasted with the good agreement we achieve in the ATLAS case. As shown in Table II, ATLAS imposes slightly different cuts than CMS. For example, ATLAS requires a harder cut of $p_T > 20\,\text{GeV}$ to veto additional jets while the CMS chooses a softer cut $p_T > 15\,\text{GeV}$. To try to gain some insight into the effects of different cuts, we systematically change the CMS cuts to ATLAS cuts and smoothly transition between the two in Table V. Our approach is to replace a cut imposed by CMS with an equivalent (or nearly equivalent) cut imposed by ATLAS. In the Table, the cuts are defined as follows:

- Cut 1 imposes the CMS lepton selection criteria and is the yardstick by which the other acceptances are measured;

- Cut 2 includes all cuts imposed by CMS and is to be directly compared with Table IV, but for $M_h = 160$ GeV;

- Cut 3 relaxes the $\not{E}_T$ cut from $\not{E}_T > 50\,\text{GeV} \implies \not{E}_T > 30\,\text{GeV}$;

- Cut 4 relaxes the invariant mass cut $12\,\text{GeV} < m_{\ell\ell} < 40\,\text{GeV} \implies 12\,\text{GeV} < m_{\ell\ell} < 300\,\text{GeV}$;

- Cut 5 relaxes azimuthal open angle $\Delta\phi_{\ell\ell} < \pi/4 \implies \Delta\phi_{\ell\ell} < \pi/2$;

- Cut 6 restores the control region of ATLAS study $M_T^C < 600\,\text{GeV}$ and removes the requirements CMS imposes on the maximum and minimum values of the transverse momenta of the leptons;

- Cut 7 removes the $Z \to \tau\tau$ background, $|m_{\tau\tau} - m_Z| < 25\,\text{GeV}$.

The threshold cuts applied at the analysis level are $p_T^j > 15$ GeV and $|\eta_j| < 2.5$, which are those applied in the CMS study. The cuts with the largest change in acceptance in going from CMS to ATLAS include Cuts 4, 5, and 6. Cut 4 was designed to eliminate Drell-Yan background in CMS where all combinations of e and μ are accepted. As ATLAS limits their analysis to the opposite flavor $e^{\pm}\mu^{\mp}$ channel, the Drell-Yan background is not much of a concern. In Cut 5, relaxing the cut on the opening angle, $\Delta\phi_{\ell\ell}$, increases acceptance. Such a strict opening angle cut is optimized more for Higgs boson searches through the WW channel near threshold where the final-state leptons are highly correlated. Of the cuts enumerated above, Cut 6 includes the largest change in cuts and is one of the last steps in going from the CMS cuts to the ATLAS cuts. It is not a surprise that there is a large shift in acceptance upon changing these cuts. In Table V we show acceptances for two different generator-level cuts on the jet p_T thresholds. We observe that the acceptances are insensitive to this change, except for the $t\bar{t}$ case.

After Cut 7 in Table V, we expect to obtain results close to those found in our ATLAS analysis, Table III. In fact, we see close agreement for the Higgs boson signal and for the WW continuum background. This agreement is not exact due to differences in the threshold cuts at the generator level and at the analysis level which are initially tailored for CMS. Our result for the $t\bar{t}$ background in the Cut 7 column is a factor of two higher than shown in Table III. We note in this connection that the physics cut for CMS requires no jets with

TABLE V: Change of the cut acceptances when we switch from the CMS cuts to the ATLAS cuts. We apply threshold cuts at the analysis level consistent with the CMS study. See the text for cut definitions. We show the acceptances for two different generator-level jet p_T thresholds of 10 and 15 GeV. For the signal process, $M_h = 160$ GeV.

process	Cut 1	Cut 2	Cut 3	Cut4	Cut5	Cut6	Cut7
$gg \to H \to WW$ ($p_T^j > 10\,\mathrm{GeV}$)	100%	11.2%	11.8%	13.7%	24.7%	33.5%	33.5%
$gg \to H \to WW$ ($p_T^j \to 15\,\mathrm{GeV}$)	100%	10.7%	11.1%	12.9%	23.2%	31.6%	31.6%
$t\bar{t}$ ($p_T^j > 10\,\mathrm{GeV}$)	100%	0.016%	0.018%	0.028%	0.068%	0.190%	0.184%
$t\bar{t}$ ($p_T^j \to 15\,\mathrm{GeV}$)	100%	0.009%	0.010%	0.020%	0.066%	0.164%	0.156%
WW ($p_T^j > 10\,\mathrm{GeV}$)	100%	1.16%	1.18%	2.02%	5.38%	10.48%	10.48%
WW ($p_T^j \to 15\,\mathrm{GeV}$)	100%	1.18%	1.19%	2.01%	5.19%	10.08%	10.08%

$|\eta| < 2.5$, whereas the quiet region for ATLAS is defined by no jets with $|\eta| < 4.8$. CMS accepts events which have jets in the region $2.5 < |\eta_j| < 4.8$ that would be vetoed by the ATLAS cuts. The factor of two is therefore understandable. Overall, we can explain how our acceptances for CMS transform into our acceptances for ATLAS. Our results are internally consistent, but we do not have an explanation for the fact that our signal and background acceptances differ from those computed by CMS only in the $t\bar{t}X$ case but compare well with all those computed by ATLAS. We use both our value and the CMS value of the $t\bar{t}X$ background to bracket our predictions of the Higgs boson search sensitivity at 7 TeV and 10 TeV in Section IV. Since this background is not dominant, the differences are not large.

IV.   HIGGS BOSON SENSITIVITY AT 7 TEV AND 10 TEV

A.   ATLAS

Having established agreement of the acceptances we compute at 14 TeV with those obtained by ATLAS, we extend our analysis to lower LHC cm energies of 7 TeV and 10 TeV. We use the ATLAS cuts shown in Table II, assuming the same cuts will apply at lower energies. Our expectations are presented in Table VI. Here, σ_{tot} denotes the NLO total cross section of the signal and backgrounds with the two intermediate W-bosons decaying into lepton pairs. We include three lepton flavors (e, μ, τ) at this stage. After taking into account

15

the detector related factors as well as the lepton selection and isolation cuts, we obtain the cross section σ_{id}, the third column in Table VI. In accord with the ATLAS 14 TeV study, we only consider the $e\mu$ final state, i.e. both $e^+\mu^-$ and $e^-\mu^+$, leading to a decay branching factor of 2/9. The optimal ATLAS cuts in Table II are imposed to further suppress the SM backgrounds, resulting in the cross section σ_{cut} (the fourth column in Table VI).

We note that, at 14 TeV, the optimal cuts work best for a Higgs boson in the mass range of 140 GeV to 180 GeV, yielding cut acceptances $\mathcal{A}_{cut}(=\sigma_{cut}/\sigma_{id})$ around 25-30%. However, the cut acceptance decreases below 20% for a heavy Higgs boson, say $m_H > 200$ GeV. This decrease is caused mainly by the cut $\Delta\phi_{\ell\ell} < \pi/2$ as the two charged leptons from the two on-shell W-bosons peak near $\Delta\phi_{\ell\ell} \sim \pi$ at high mass.

After imposing all cuts we find that the signal is below the backgrounds where the WW continuum is the leading background and W+jets is the sub-leading background. In Fig. 3, we show the distribution in $\ell^+\ell^-$ $\not{E}_T$ cluster transverse mass,

$$M_T^C \equiv \sqrt{p_T^2(\ell\ell) + m^2(\ell\ell)} + \not{E}_T,$$

for the Higgs boson signal and three principal backgrounds at LHC energies of 7, 10, and 14 TeV. The Wc background is most important at low values of M_T^C while the WW continuum tends to be important at large values of M_T^C. The top quark pair background is quite small owing to the jet veto cut.

At 14 TeV the signal to background ratio ($S/B \equiv \sigma_s/\sigma_B$) increases from 18% to 28% when the Higgs boson mass increases from 140 GeV to 180 GeV, but it decreases to 13% for a 200 GeV Higgs boson. The decrease is the net effect of the cut acceptance and branching ratio $Br(H \to WW)$. The latter drops from 94% to 73% when the Higgs boson mass increases from 180 GeV to 200 GeV, owing to opening of the ZZ mode. We present the significance in the last column of Table VI assuming an integrated luminosity ($\mathcal{L}$) of 1 fb^{-1}.

Upon lowering the cm energy we find that the cut acceptances increase for both the signal and backgrounds. The signal cross section decreases more than the WW background cross section. As a result, the S/B ratios at 10 TeV and 7 TeV are less than those at 14 TeV. The lower cm energy, the smaller S/B ratio and the signal significance. The latter is defined as

$$\frac{S}{\sqrt{B}} = \frac{\sigma_S}{\sqrt{\sigma_B}} \times \sqrt{\mathcal{L}}. \tag{11}$$

TABLE VI: Discovery potential at the Large Hadron Collider with the ATLAS cuts imposed. Here, σ_{tot} denotes the total cross section (pb) of the signal ($gg \to H \to WW$) and backgrounds, including the W-boson decay branching ratio into the three flavors of leptons. σ_{id} is the cross section after the lepton reconstruction and isolation, σ_{cut} presents the cross section after all ATLAS cuts are imposed. $\mathcal{A}_{cut}$ is the cut acceptance, defined as σ_{cut}/σ_{id}.

14 TeV	σ_{tot}(pb)	σ_{id}(fb)	σ_{cut}(fb)	$\mathcal{A}_{\text{cut}}$	σ_S/σ_B	$\sigma_S/\sqrt{\sigma_B}$
$m_H = 140\,\text{GeV}$	1.50	125	30.6	24.5%	18.2%	2.36
$m_H = 160\,\text{GeV}$	2.19	208	61.4	29.5%	36.7%	4.75
$m_H = 180\,\text{GeV}$	1.85	183	47.9	26.2%	28.6%	3.70
$m_H = 200\,\text{GeV}$	1.21	110	21.8	19.8%	13.0%	1.68
$t\bar{t} + (0,1,2)j$	89.7	6350	4.64	0.073%	-	-
$WW + (0,1,2)j$	12.7	737	87.0	11.8%	-	-
$Wc + (0,1,2,3,4)j$	2820	945	75.8	8.02%	-	-
10 TeV	σ_{tot}(pb)	σ_{id}(fb)	σ_{cut}(fb)	$\mathcal{A}_{\text{cut}}$	σ_S/σ_B	$\sigma_S/\sqrt{\sigma_B}$
$m_H = 140\,\text{GeV}$	0.773	63.8	16.7	26.2%	13.3%	1.49
$m_H = 160\,\text{GeV}$	1.12	107	33.9	31.7%	26.9%	3.02
$m_H = 180\,\text{GeV}$	0.939	92.5	24.8	26.8%	19.7%	2.21
$m_H = 200\,\text{GeV}$	0.610	55.5	11.3	20.4%	8.98%	1.00
$t\bar{t} + (0,1,2)j$	41.5	3070	2.46	0.080%	-	-
$WW + (0,1,2)j$	7.99	506	66.3	13.1%	-	-
$Wc + (0,1,2,3,4)j$	1670	571	57.1	10.0%	-	-
7 TeV	σ_{tot}(pb)	σ_{id}(fb)	σ_{cut}(fb)	$\mathcal{A}_{\text{cut}}$	σ_S/σ_B	$\sigma_S/\sqrt{\sigma_B}$
$m_H = 140\,\text{GeV}$	0.397	31.5	8.66	27.5%	9.9%	0.923
$m_H = 160\,\text{GeV}$	0.563	53.1	17.3	32.5%	19.8%	1.85
$m_H = 180\,\text{GeV}$	0.458	44.9	12.8	28.6%	14.6%	1.37
$m_H = 200\,\text{GeV}$	0.291	26.6	5.93	22.3%	6.76%	0.633
$t\bar{t} + (0,1,2)j$	17.6	1340	1.34	0.100%	-	-
$WW + (0,1,2)j$	4.73	337	48.2	14.3%	-	-
$Wc + (0,1,2,3,4)j$	905	322	38.0	11.8%	-	-

TABLE VII: Similar to Table VI, discovery potential at the Large Hadron Collider with CMS cuts imposed for 1 fb^{-1}. We provide two sets of values for the $t\bar{t}X$ background, our computed value and in parentheses the value attributed to CMS.

14 TeV	σ_{tot}(pb)	σ_{id}(fb)	σ_{cut}(fb)	$\mathcal{A}_{\text{cut}}$	σ_S/σ_B	$\sigma_S/\sqrt{\sigma_B}$
$m_H = 140\,\text{GeV}$	1.50	160	7.15	4.47%	36.0% (27.9%)	1.60 (1.41)
$m_H = 160\,\text{GeV}$	2.19	340	37.7	11.1%	190% (147%)	8.46 (7.45)
$m_H = 180\,\text{GeV}$	1.85	309	17.8	5.75%	89.6% (69.5%)	3.99 (3.52)
$m_H = 200\,\text{GeV}$	1.21	229	4.23	1.85%	21.3% (16.5%)	0.949 (0.836)
$t\bar{t} + (0,1,2)j$	89.7	13400	2.28 (8.04)	0.017% (0.06%)	-	-
$WW + (0,1,2)j$	12.7	913	11.3	1.24%	-	-
$Wc + (0,1,2,3,4)j$	2820	3430	6.28	0.183%	-	-

10 TeV	σ_{tot}(pb)	σ_{id}(fb)	σ_{cut}(fb)	$\mathcal{A}_{\text{cut}}$	σ_S/σ_B	$\sigma_S/\sqrt{\sigma_B}$
$m_H = 140\,\text{GeV}$	0.773	82.0	4.23	5.17%	29.6% (26.3%)	1.12 (1.05)
$m_H = 160\,\text{GeV}$	1.12	173	19.6	11.4%	137% (122%)	5.19 (4.88)
$m_H = 180\,\text{GeV}$	0.939	161	9.63	5.98%	67.4% (59.8%)	2.55 (2.40)
$m_H = 200\,\text{GeV}$	0.610	116	2.24	1.93%	15.7% (13.9%)	0.593 (0.558)
$t\bar{t} + (0,1,2)j$	41.5	6500	0.715 (2.54)	0.011% (0.039%)	-	-
$WW + (0,1,2)j$	7.99	659	8.17	1.24%	-	-
$Wc + (0,1,2,3,4)j$	1670	1930	5.40	0.280%	-	-

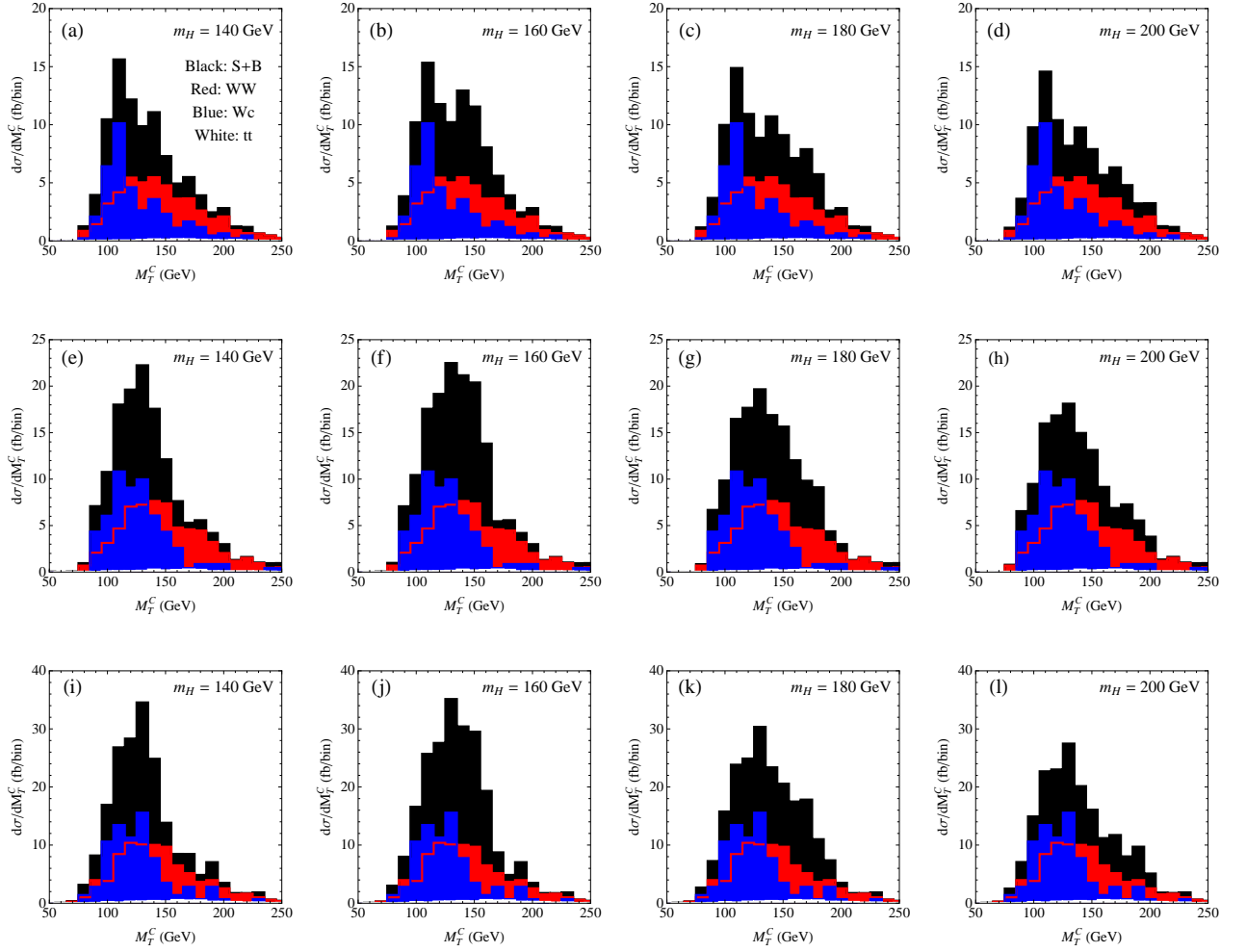| 7 TeV	σ_{tot}(pb)	σ_{id}(fb)	σ_{cut}(fb)	$\mathcal{A}_{\text{cut}}$	σ_S/σ_B	$\sigma_S/\sqrt{\sigma_B}$
$m_H = 140\,\text{GeV}$	0.397	39.1	1.99	5.08%	23.2% (21.6%)	0.680 (0.655)
$m_H = 160\,\text{GeV}$	0.563	88.4	10.6	12.0%	124% (115%)	3.62 (3.49)
$m_H = 180\,\text{GeV}$	0.458	79.3	4.82	6.08%	56.3% (52.2%)	1.65 (1.59)
$m_H = 200\,\text{GeV}$	0.291	57.1	1.17	2.05%	13.7% (12.7%)	0.400 (0.385)
$t\bar{t} + (0,1,2)j$	17.6	2890	0.260 (0.925)	0.009% (0.032%)	-	-
$WW + (0,1,2)j$	4.72	428	5.31	1.24%	-	-
$Wc + (0,1,2,3,4)j$	905	1050	2.99	0.285%	-	-

FIG. 3: Distributions of the cluster transverse mass M_T^C for 7 TeV (a-d), 10 TeV (e-h) and 14 TeV (i-l), where the black region denotes the signal plus background while the red, blue and white regions denote the WW, Wc and $t\bar{t}$ backgrounds, respectively. Here, all ATLAS cuts are imposed.

B. CMS

The results of our analysis of CMS expectations at LHC cm energies of 7 TeV and 10 TeV are shown in Table VII. We use the CMS cuts shown in Table II, assuming the same cuts will apply at lower energies. Here, σ_{tot} denotes the NLO total cross section of the signal and backgrounds, including the lepton-pair branching fractions for decay of the two intermediate W-bosons into three lepton flavors (e, μ, τ). The identified cross section σ_{id} is obtained from σ_{tot} after lepton selection and isolation cuts are imposed on the events we generate, as defined

in Sec. III. Recall that CMS averages over all decay modes including $ee, \mu\mu$, and $e\mu$. We also include the CMS trigger efficiencies ("L1 + HLT") in σ_{id}. Since we have no way of computing these efficiencies, we assume that they are independent of the cm energy and use the values in the CMS PPR (c.f. Fig. 10.12 on page 1276). For the signal, the value of the trigger efficiency depends on the Higgs boson mass and varies from 0.50 to 0.63 for the range of masses considered here. For the backgrounds, the corresponding efficiencies are 0.67 for $t\bar{t}$ and 0.52 for WW.

The CMS analysis cuts in Table II are imposed, resulting in the cross section σ_{cut} (the fourth column in Table VII). For the $t\bar{t}$ background, we list two values of σ_{cut}: one corresponds to the value obtained from our calculation, while the other in parentheses is the larger value quoted in the CMS PPR. As pointed out above, the two differ by roughly a factor of 3.5 at a cm energy of 14 TeV. Since we are unsure of the cause of this discrepancy, we give results for both cut efficiencies as a way of bracketing our uncertainty. At the lower cm energies, we simply rescale our computed value of σ_{cut} for the $t\bar{t}$ background by a factor of 3.5 to obtain what we assume CMS would obtain.

We include a W+jets background contribution (computed as $W+c$) in addition to $t\bar{t}$ and WW. This channel can provide a background comparable to (or even larger) than $t\bar{t}$. Since CMS did not include this background in their analysis, there is no quote for the "L1+HLT" trigger efficiency for this channel. The numbers shown in Table VII for W+jets assume perfect efficiency and, thus, are an overestimate of the true rate.

For the signal, the cut acceptances $\mathcal{A}_{cut}(= \sigma_{cut}/\sigma_{id})$ for CMS tend to be smaller than for ATLAS, in the 5 - 10% range versus 25-30% at 14 TeV However, the signal to background fractions are higher, exceeding 100% at $m_H = 160$ GeV. Our calculated signal significance is found in the last column of Table VII for an assumed integrated luminosity ($\mathcal{L}$) of 1 fb^{-1}. For $m_H = 160$ GeV, we find a signal significance of 7.4 to 8 σ at 14 TeV, depending on how the $t\bar{t}$ background is estimated. This value drops to about 5 σ at 10 TeV and to about 3 σ at 7 TeV. The significance drops off on both sides of $m_H = 160$ GeV at all energies.

We find reasonable agreement of our predicted significance at 14 TeV to that of CMS for $m_H = 160$ GeV. If the $gg \rightarrow WW$ contribution is omitted, the total signal and background $(t\bar{t} + WW)$ cross sections in the CMS PPR (after all cuts) are $\sigma_S = 42$ fb and $\sigma_B = 21.8$ fb, and the signal significance is then $\sigma_S/\sqrt{\sigma_B} = 9.00$. If we remove the $W + c$ background from our analysis, our total cross sections (after all cuts) are $\sigma_S = 35.4$ fb and $\sigma_B = 19.3$ fb,

and our signal significance is $\sigma_S/\sqrt{\sigma_B} = 8.05$. The difference between the two expectations, roughly $\sim 10\%$, seems to us well within the theoretical uncertainties. The agreement at 14 TeV lends credibility to our estimates at the lower energies.

There are uncertainties associated with our values of the cut acceptance $\mathcal{A}_{cut}$ and corresponding signal significance $\sigma_S/\sqrt{\sigma_B}$ in Tables VI and VII. The most obvious uncertainties can be traced to the choice of PDFs and the renormalization and factorization scales. We also use inclusive NLO K factors, rather than K factors that apply in the restricted part of phase space after analysis cuts are applied. Some of these uncertainties are reduced in ratios such as $\mathcal{A}_{cut}$. The uncertainties presented in Figs. 4 – 6 are based solely on the statistics of the samples of events that we generate and are no doubt an underestimate of the full uncertainty.

C. ATLAS and CMS Comparison

Comparing Table VII and Table VI, we see that considerably larger signal significance at $m_H = 160$ GeV is obtained with the CMS cuts. We attribute this difference to the effects of the different analysis cuts in the two cases, particularly the cuts on m_{ll} and $\Delta\phi_{ll}$. The advantage of these cuts diminishes for values of m_H below and above 160 GeV.

In Fig. 4, we display our computed signal significance for 1 fb^{-1} of integrated luminosity as a function of Higgs boson mass. Results are shown at three values of the LHC energy based on the ATLAS and CMS cuts. Except at $m_H = 160$ GeV, the expectations are similar for the two sets of cuts. At $m_H = 160$ GeV, we see that ATLAS may achieve nearly 5 σ significance with 1 fb^{-1} at 14 TeV, and about 3 σ and almost 2 σ at 10 TeV and 7 TeV, respectively. The corresponding CMS numbers are roughly 8 σ, 5 σ, and 3.5 σ at 14, 10, and 7 TeV, respectively.

In Fig. 5 we present our calculation of the integrated luminosity required to achieve 5σ discovery as a function of m_H. In the ATLAS case, we see that 1 fb^{-1} is essentially sufficient for $m_H = 160$ GeV at 14 TeV, but increases to about 3 fb^{-1} and 8 fb^{-1} are needed at 10 and 7 TeV, respectively. With the CMS analysis cuts, 1 fb^{-1} is more than sufficient for $m_H = 160$ GeV at 14 TeV, and is sufficient at 10 TeV, but an increase to about 2 fb^{-1} is needed at 7 TeV.

To reproduce the significance at 14 TeV, a larger luminosity is needed at the lower energies
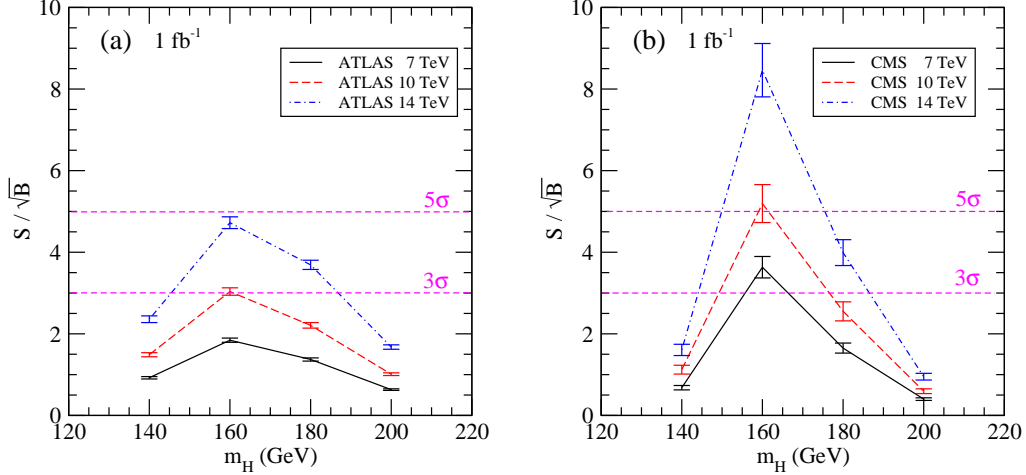
FIG. 4: Signal significance as a function of m_H at ATLAS and CMS with $1\,\mathrm{fb}^{-1}$ luminosity.
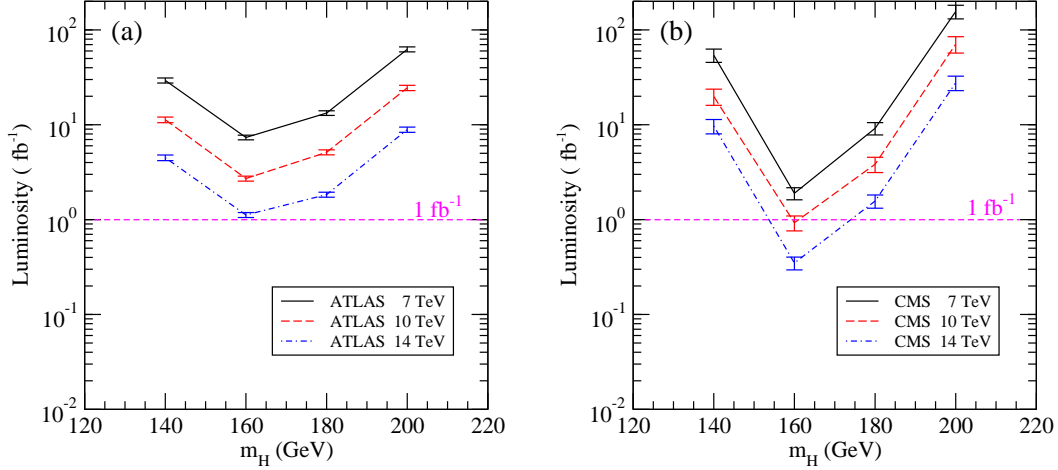

FIG. 5: Integrated luminosity required for 5σ discovery as a function of m_H in the ATLAS and CMS cases.

to compensate the additional suppression of signal cross section compared to the background cross section. The enhancement factor of the luminosity is

$$\frac{\mathcal{L}_i}{\mathcal{L}_{14}} = \left[\left(\frac{\sigma_S}{\sqrt{\sigma_B}} \right)_{14} \Big/ \left(\frac{\sigma_S}{\sqrt{\sigma_B}} \right)_i \right]^2. \tag{12}$$

For the two experiments, Fig. 6 shows the factors by which the luminosity must be increased at lower energies to discover a Higgs boson with the same significance as at 14 TeV. Over the range of Higgs boson masses considered, one would need to increase $\mathcal{L}$ by a factor of roughly 2.5 at 10 TeV for the cuts we associate with ATLAS and CMS. At 7 TeV, the factor is ~ 5 in the CMS case and ~ 6.5 in the ATLAS case. These predictions are
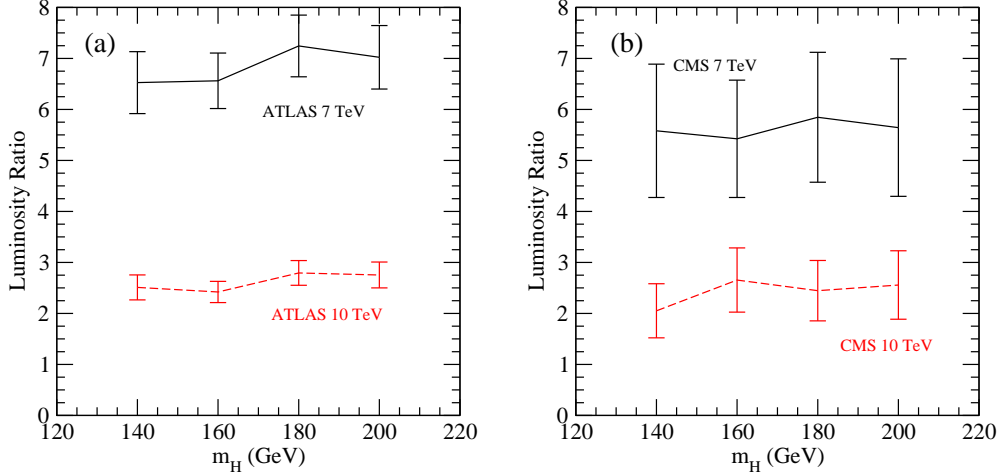
FIG. 6: Factors by which the integrated luminosity must be increased at LHC energies of 7 and 10 TeV to achieve the same signal significance as at 14 TeV.

relatively unaffected by the different values of $\mathcal{A}_{cut}$ for the $t\bar{t}$ background in the CMS case. The uncertainties are about 9% at 10 TeV and 8.6% at 7 TeV in the ATLAS case and close to 25% for both energies in the CMS case. The more restrictive analysis cuts in the CMS case (*c.f.* our Table II) lead to a smaller event sample and therefore larger statistical uncertainties.

V.   EXCLUSIONS – TEVATRON AND LHC

The $H \to WW$ and other decay modes are used in the recent CDF and D0 combined fit of Tevatron data to exclude the mass range $163\,\text{GeV} < m_H < 166\,\text{GeV}$ at 95% C. L. [6]. The integrated luminosity differs among the various production and decay modes in the Tevatron study, ranging from 2.0 fb^{-1} to 5.4 fb^{-1}. In Fig. 7, we sketch the current combined Tevatron limit on Higgs boson production in units of the SM cross section, under the assumption of an exclusion. To estimate naively the sensitivity that Tevatron studies will achieve with 10 fb^{-1} by perhaps the end of 2011, we multiply the current expected limit by $\sqrt{\mathcal{L}_{current}/\mathcal{L}_{projected}}$. We choose to scale the expected limit rather than the observed limit since it is based on a larger event sample and less subject to statistical fluctuations. Scaling the observed limit is more sensitive to the fluctuations present in observed events, expected to average out if no signal is present. We provide two possible extrapolations, from either 2.0 fb^{-1} or 5.4 fb^{-1} of integrated luminosity. The Tevatron analyses of the $WW \to \ell^+\nu\ell^-\bar{\nu}$ channel
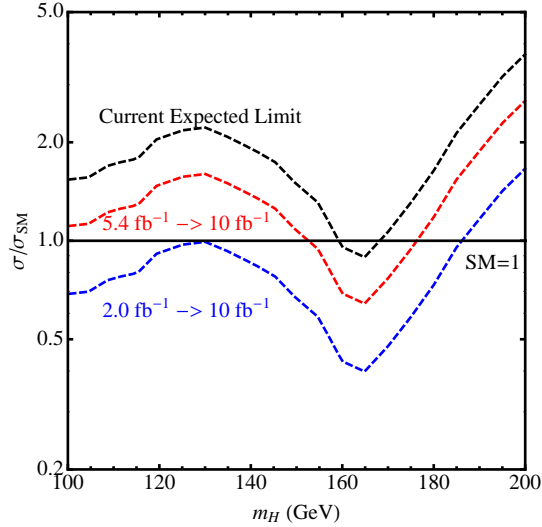
FIG. 7: Current 95% exclusion limits for a SM Higgs boson from the combined CDF and D0 study, and projected exclusion limits with 10 fb^{-1} of integrated luminosity at the Tevatron.

include up to 5.4 fb^{-1} of data. Therefore, the limit for Higgs boson masses above 160 GeV is expected to follow the projected 5.4 fb^{-1} $\to$ 10 fb^{-1} curve, yielding an exclusion of the range 153 to 177 GeV (based on statistics alone). A detailed analysis of a combined Tevatron exclusion limit with up to 4.2 fb^{-1} of integrated luminosity [33] is provided in Ref. [34] in which individual channels are scaled by the respective ratios $\sqrt{\mathcal{L}_{current}/\mathcal{L}_{projected}}$ and then combined. We observe that the projected 10 fb^{-1} exclusion limit in Ref. [34] and our 5.4 fb^{-1} $\to$ 10 fb^{-1} projection in Fig. 7 are almost identical, supporting the validity of the projections in the relevant mass range $\sim$ 150 to $\sim$ 180 GeV . An increase in efficiency can improve the mass exclusion limits [34].

To compare with the expected sensitivity of the Tevatron, our LHC results can be recast as limits on the Higgs boson production cross section assuming no signal is found. Based on Poisson statistics, we determine the signal cross section at the LHC that is consistent at 95% C.L. with the calculated background for the ATLAS and CMS cuts Refs. [1] and [2] (using our calculation of $t\bar{t}$). These cross sections can be divided by the SM Higgs boson production cross sections to obtain the limits shown in Fig. 8. The results show that with 1 fb^{-1} of integrated luminosity at 7 TeV, CMS may be able to exclude m_H values of 160 and 180 GeV (and perhaps points in between), while ATLAS may be able to exclude 160 GeV. The difference between the two experiments is traced to the different set of analysis cuts,
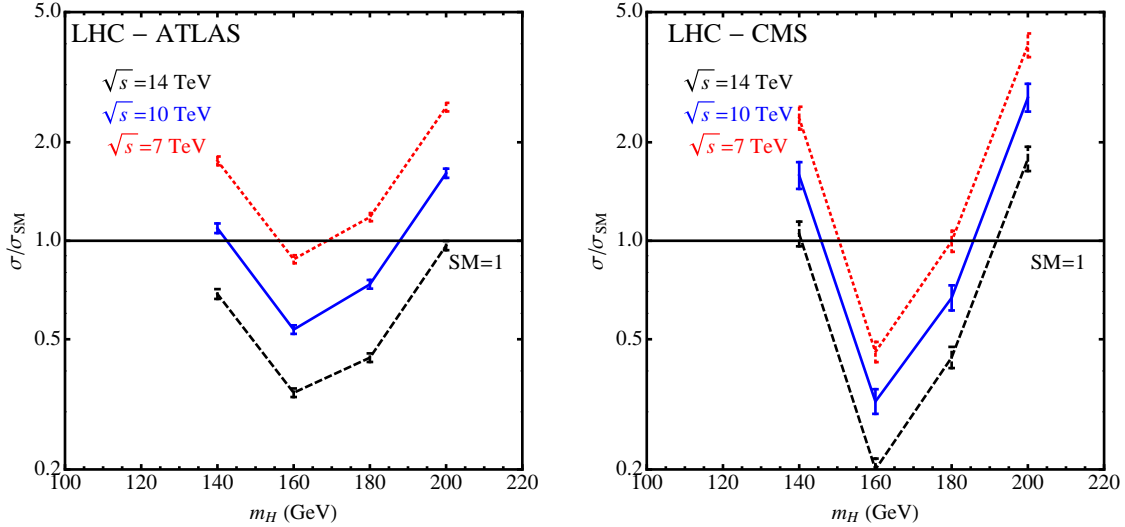
FIG. 8: Estimated exclusion limits for a SM Higgs boson produced via gluon fusion and decaying via $WW \to llX$ with 1 fb^{-1} of integrated luminosity for the ATLAS and CMS experiments for three LHC energies.

described in Refs. [1] and [2] and summarized in our Table II. Figure 8 suggests that the exclusion range at the LHC may extend below 160 GeV. However, since our calculations are done at fixed values of the Higgs boson mass, we refrain from making statements for values other than those at which we have explicit results. The figures show that with 1 fb^{-1} of integrated luminosity at 7 TeV the ATLAS exclusion range should be comparable to the current Tevatron exclusion range, and that the CMS exclusion range should be comparable to a Tevatron study with 10 fb^{-1}. Comparison of Figs. 7 and 8 indicates that the Tevatron experiments should remain competitive through 2011 and perhaps beyond provided they achieve analyses based on 10 fb^{-1} of integrated luminosity.

VI. CONCLUSIONS

In this paper, we provide Higgs boson discovery prospects for early LHC running at energies of 7 and 10 TeV for the $gg \to H \to W^+W^- \to \ell^+\ell^- + \not{E}_T$ channel. Our estimates of the Higgs boson signal and backgrounds are obtained from parton-level simulations. We apply the same cuts used by the CMS [2] and ATLAS [1] collaborations, and we verify that our acceptances for the signal, W^+W^- and $W^\pm + n$ jets channels agree with those of CMS and ATLAS. Our acceptance for the $t\bar{t}$ process matches well when compared to

the ATLAS results, but it is in less good agreement with the CMS results. This difference may be understood in terms of the low jet p_T threshold taken by CMS where a full parton shower simulation may be necessary. We obtain good agreement with the ATLAS and CMS collaboration estimates of signal significance at 14 TeV for Higgs boson masses near $m_H = 160$ GeV.

With 1 fb^{-1} of integrated luminosity at $\sqrt{s} = 14$ TeV, using the same analysis cuts as the collaborations, we conclude that a SM Higgs boson with mass $m_H = 160$ GeV can be discovered at about the 5σ level with the ATLAS cuts imposed and about 8σ with the CMS cuts imposed. At $\sqrt{s} = 10$ TeV, a 3 σ evidence is possible in the ATLAS case and about 5.2 σ in the CMS case for the same integrated luminosity. At $\sqrt{s} = 7$ TeV, the numbers drop to about 2 σ in the ATLAS case and about 3.6 σ in the CMS case.

It is important to bear in mind that our different stated expectations for the two experiments arise from the different analysis cuts in the two cases, summarized here in Table II, particularly the cuts on the dilepton invariant mass m_{ll} and on the difference $\Delta\phi_{ll}$ in the azimuthal angles of the two leptons. The CMS analysis cuts are more restrictive, tuned more to the region near 160 GeV, a reason for the greater signal significance and larger statistical uncertainty in our CMS simulations.

Integrated luminosities of 8 fb^{-1} and 3 fb^{-1} are needed in the ATLAS case at 7 and 10 TeV, respectively, for 5σ level discovery of a standard model Higgs boson of mass $m_H = 160$ GeV in the $gg \to H \to W^+W^- \to \ell^+\ell^- + \not{E}_T$ channel. In the CMS case, the numbers are 2 fb^{-1} and 1 fb^{-1} at 7 and 10 TeV, respectively, for 5σ level discovery. Larger samples would be needed for masses as low as $m_H = 140$ GeV or above $m_H = 180$ GeV.

In the range 140 GeV $< m_H <$ 200 GeV, to achieve the same signal sensitivity as at 14 TeV with 1 fb^{-1} of integrated luminosity, we estimate that a factor of 6 to 7 more luminosity is required at 7 TeV for the analysis cuts proposed by ATLAS, and a factor of about 5 in the CMS case. At 10 TeV, the factor is in the range ~ 2.5 for both experiments.

The acceptances of the Higgs boson signal and dominant backgrounds across the mass range we consider generally increase as the center of mass energy is reduced. As the cm energy is decreased, the signal cross section is suppressed more than the irreducible background from the WW continuum. Therefore, more integrated luminosity at a lower cm energy is needed to restore the same significance. While it is likely that cuts can be tuned to improve the expected signal significance at 7 TeV, it also seems likely that Higgs boson dis-

covery in the $H \to W^+W^- \to \ell^+\ell^- + \not{E}_T$ mode will require more luminosity than currently anticipated.

Under the assumption that no signal is found, we may restate our results as 95% exclusion limits on Higgs boson production in gg fusion followed by decay into the WW dilepton mode. Our results show that with 1 fb^{-1} of integrated luminosity at 7 TeV, CMS may be able to exclude m_H values of 160 and 180 GeV (and perhaps points in between), while ATLAS may be able to exclude 160 GeV. Comparison of Figs. 7 and 8 indicates that the Tevatron experiments should remain competitive in the near future provided they achieve analyses based on 10 fb^{-1} of integrated luminosity.

Acknowledgments

[1] ATLAS Technical Design Report, G. Aad *et al.*, (2009), arXiv:0901.0512.

[2] CMS Technical Design Report Volume II:, `http://cmsdoc.cern.ch/cms/cpt/tdr/ptdr2_final.pdf` .

[3] *Summary of the LHC Performance Workshop - Chamonix*, 2010, `http://indico.cern.ch/conferenceOtherViews.py?view=standard&confId=83135`.

[4] J. F. Gunion, H. Haber, G. Kane, and S. Dawson, *The Higgs Hunter's Guide* (Westview Press, 2000).

[5] A. Djouadi, Phys. Rept. **457**, 1 (2008), arXiv:hep-ph/0503172.

[6] CDF and D0 Collaborations, (2009), arXiv:0911.3930.

[7] Z. Sullivan and E. L. Berger, Phys. Rev. **D74**, 033008 (2006), arXiv:hep-ph/0606271.

[8] Z. Sullivan and E. L. Berger, Phys. Rev. **D78**, 034030 (2008), arXiv:0805.3720.

[9] S. Dawson, Nucl. Phys. **B359**, 283 (1991).

[10] R. V. Harlander and W. B. Kilgore, Phys. Rev. Lett. **88**, 201801 (2002), arXiv:hep-ph/0201206.

[11] C. Anastasiou and K. Melnikov, Nucl. Phys. **B646**, 220 (2002), arXiv:hep-ph/0207004.

[12] V. Ravindran, J. Smith, and W. L. van Neerven, Nucl. Phys. **B665**, 325 (2003), arXiv:hep-ph/0302135.

[13] A. Djouadi, M. Spira, and P. M. Zerwas, Phys. Lett. **B264**, 440 (1991).

[14] D. Graudenz, M. Spira, and P. M. Zerwas, Phys. Rev. Lett. **70**, 1372 (1993).

[15] A. Djouadi and P. Gambino, Phys. Rev. Lett. **73**, 2528 (1994), arXiv:hep-ph/9406432.

[16] U. Aglietti, R. Bonciani, G. Degrassi, and A. Vicini, Phys. Lett. **B595**, 432 (2004), arXiv:hep-ph/0404071.

[17] G. Degrassi and F. Maltoni, Phys. Lett. **B600**, 255 (2004), arXiv:hep-ph/0407249.

[18] S. Actis, G. Passarino, C. Sturm, and S. Uccirati, Phys. Lett. **B670**, 12 (2008), arXiv:0809.1301.

[19] C. Anastasiou, R. Boughezal, and F. Petriello, JHEP **04**, 003 (2009), arXiv:0811.3458.

[20] MCFM, `http://mcfm.fnal.gov/` .

[21] P. M. Nadolsky *et al.*, Phys. Rev. **D78**, 013004 (2008), arXiv:0802.0007.

[22] E. L. Berger and Q.-H. Cao, Phys. Rev. **D81**, 035006 (2010), arXiv:0909.3555.

[23] T. Sjostrand, S. Mrenna, and P. Skands, Comput. Phys. Commun. **178**, 852 (2008), arXiv:arXiv:0710.3820 [hep-ph].

[24] G. Corcella *et al.*, (2002), arXiv:hep-ph/0210213.

[25] S. Frixione and B. R. Webber, JHEP **06**, 029 (2002), arXiv:hep-ph/0204244.

[26] S. Frixione and B. R. Webber, (2006), arXiv:hep-ph/0612272.

[27] S. Frixione, P. Nason, and C. Oleari, JHEP **11**, 070 (2007), arXiv:0709.2092.

[28] F. Maltoni and T. Stelzer, JHEP **02**, 027 (2003), arXiv:hep-ph/0208156.

[29] M. L. Mangano, M. Moretti, F. Piccinini, R. Pittau, and A. D. Polosa, JHEP **07**, 001 (2003), arXiv:hep-ph/0206293.

[30] C. Anastasiou, G. Dissertori, M. Grazzini, F. Stockli, and B. R. Webber, JHEP **08**, 099 (2009), arXiv:0905.3529.

[31] C. Anastasiou, G. Dissertori, F. Stockli, and B. R. Webber, JHEP **03**, 017 (2008), arXiv:0801.2682.

[32] M. Dittmar and H. K. Dreiner, Phys. Rev. **D55**, 167 (1997), arXiv:hep-ph/9608317.

[33] CDF and D0, (2009), arXiv:0903.4001.

[34] P. Draper, T. Liu, and C. E. M. Wagner, Phys. Rev. **D80**, 035025 (2009), arXiv:0905.4721.